Electronic Supplementary Information

Acid induced acetylacetonato replacement in biscyclometalated iridium(III) complexes

Yanfang Li,[a,b] Yang Liu *[a,c] and Ming Zhou* [a,c]

[a] Suzhou Institute of Nano-Tech and Nano-Bionics, Chinese Academy of Sciences, 398 Ruoshui Road, Suzhou Industrial Park, Jiangsu, 215123, P. R. China.

[b] Graduate School of the Chinese Academy of Sciences. Beijing, 100049, P. R. China

[c] SunaTech Inc. bioBAY, Suzhou Industrial Park, Jiangsu, 215123, P. R. China

E-mail: mzhou2007@sinano.ac.cn
yliu2007@sinano.ac.cn

List of Scheme and Figures

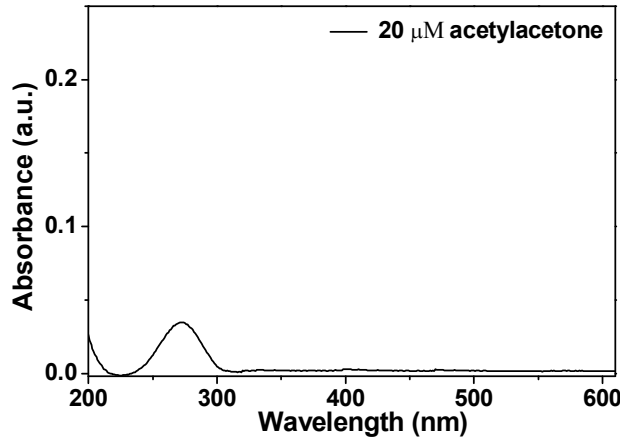

Fig. S1. UV-Vis spectrum of acetylacetone (20 μM) in CH_3CN solution

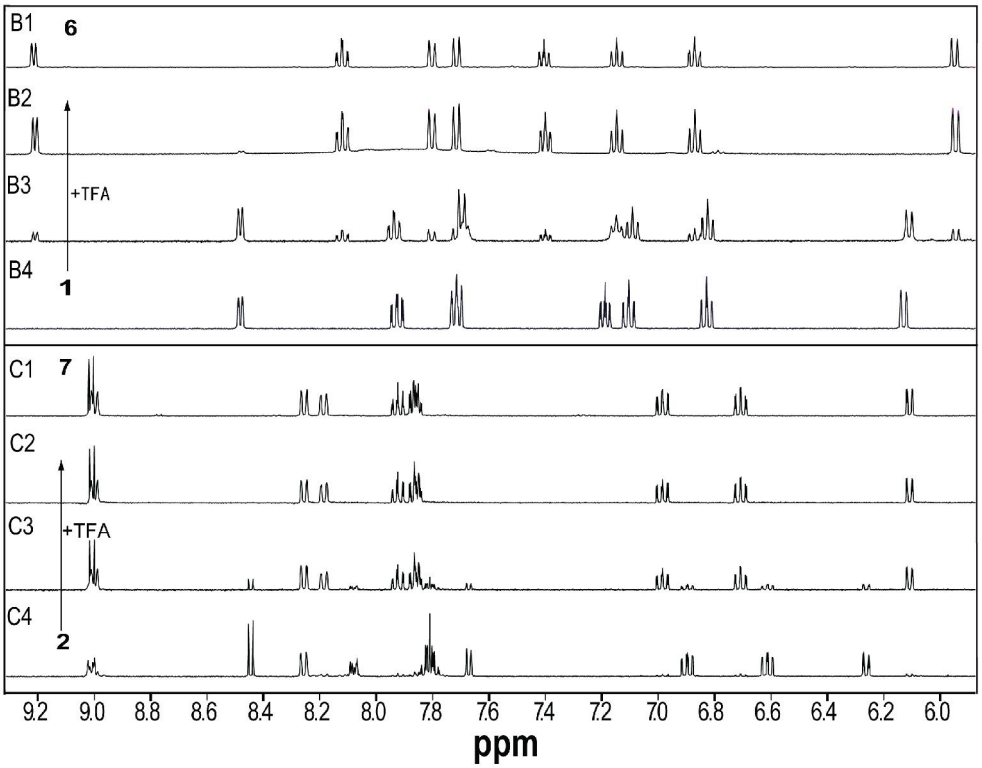

Fig. S2. ^{1}H NMR investigation of the transition from Ir(L)$_2$(acac) to [Ir(L)$_2$(MeCN)$_2$][OTf] upon the addition of TFA-*d* of 2 and 3 equiv. B: from **1** to **6**; C: from **2** to **7**; (all complexes dissolved in CD_3CN, *ca.* 4 mM).

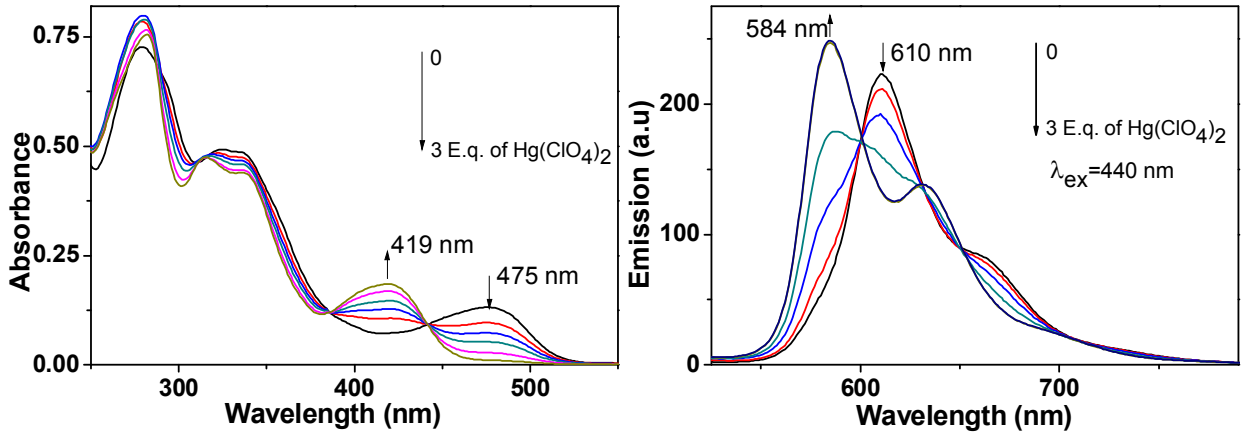

Fig. S3. UV-Vis and emission spectra of $Ir(btp)_2acac$ (20 μM) in CH_3CN solution with/without Hg^{2+}.

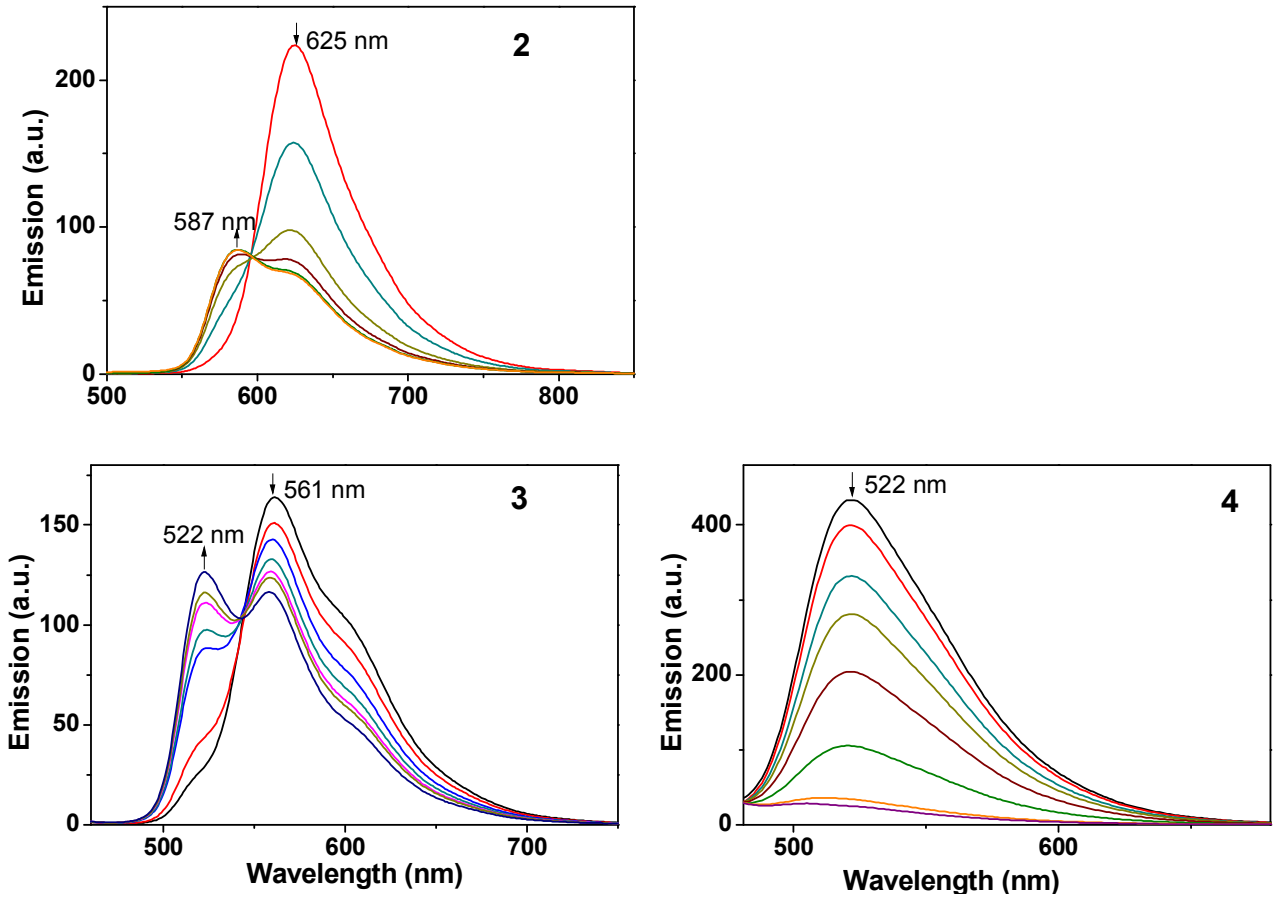

Fig. S4. Emission spectra of complex **2-4** (20 μM) in CH_3CN solution upon addition of different amounts $Hg(ClO_4)_2$.

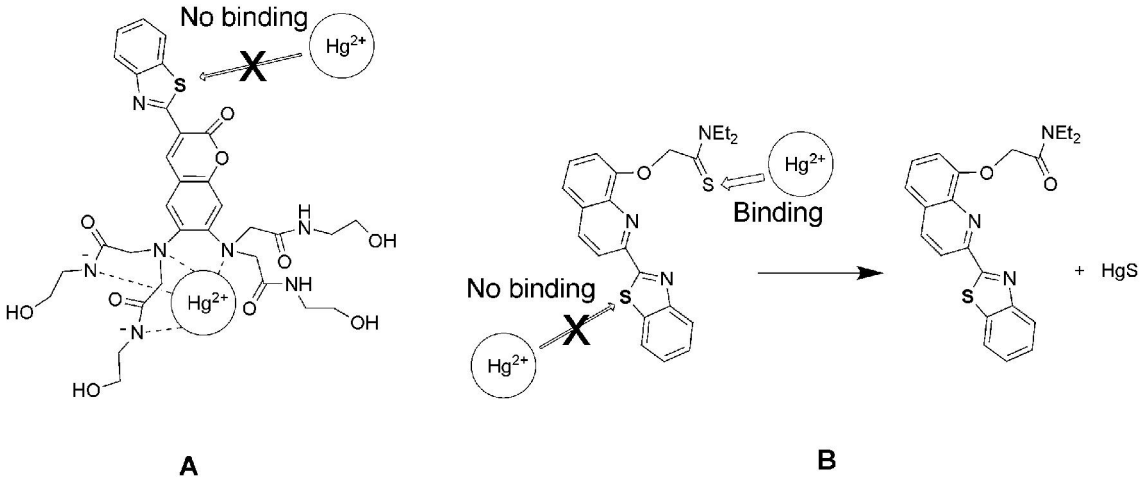

Scheme S1. Hg^{2+} sensing mechanisms proposed in Ref. 23 (A) and Ref. 24 (B).

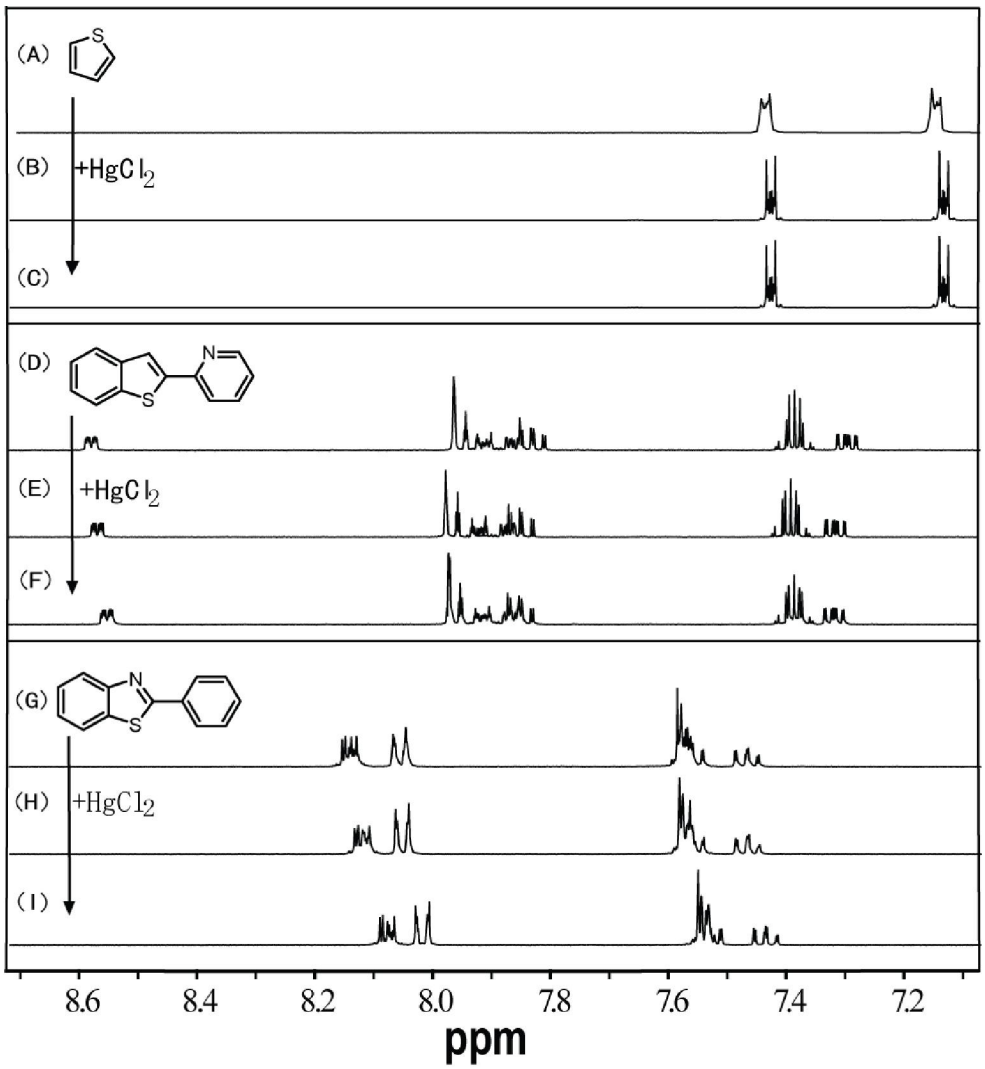

Fig. S5. ^1H NMR studies on the sufur-containing compounds (20 mM in CD_3CN) upon the addition of $HgCl_2$. (A) thiophene, (B) thiophene plus 1 equiv. of $HgCl_2$ and (C) thiophene plus 2 equiv. of $HgCl_2$; (D) btp, (E) btp plus 1 equiv. of $HgCl_2$ and (F) btp plus 2 equiv. of $HgCl_2$; (G) bt, (H) bt plus 1 equiv. of $HgCl_2$ and (I) bt plus 2 equiv. of $HgCl_2$.

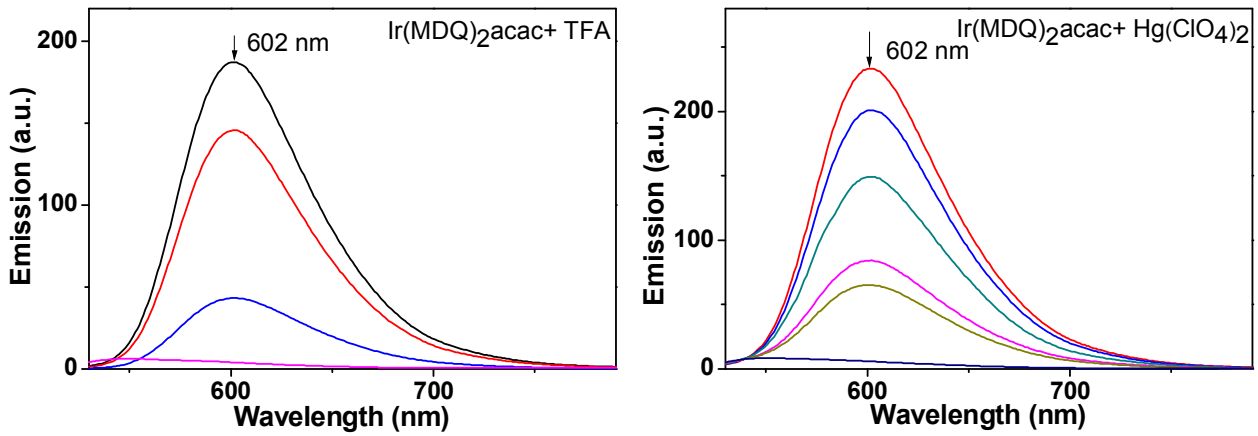

Fig. S6. Emission spectra of complex $Ir(MDQ)_2acac$ (20 μM) in CH_3CN solution upon addition of different amounts TFA and $Hg(ClO_4)_2$. λ_{ex} = 445 nm

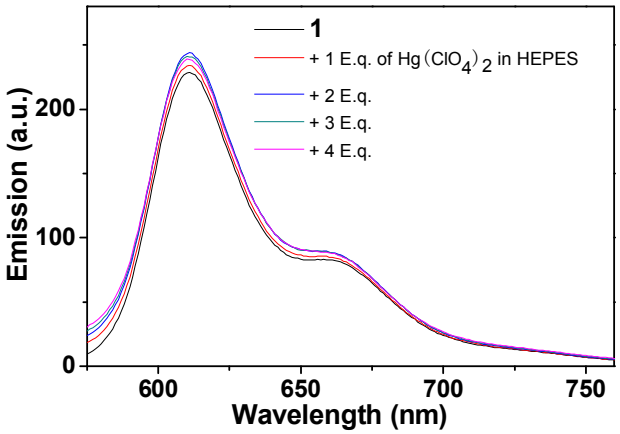

Fig. S7. Emission spectra of **1** (20 μM) in MeCN solution by addition of different amounts of $Hg(ClO_4)_2$ in HEPES aqueous solution (λ_{ex} = 440 nm)

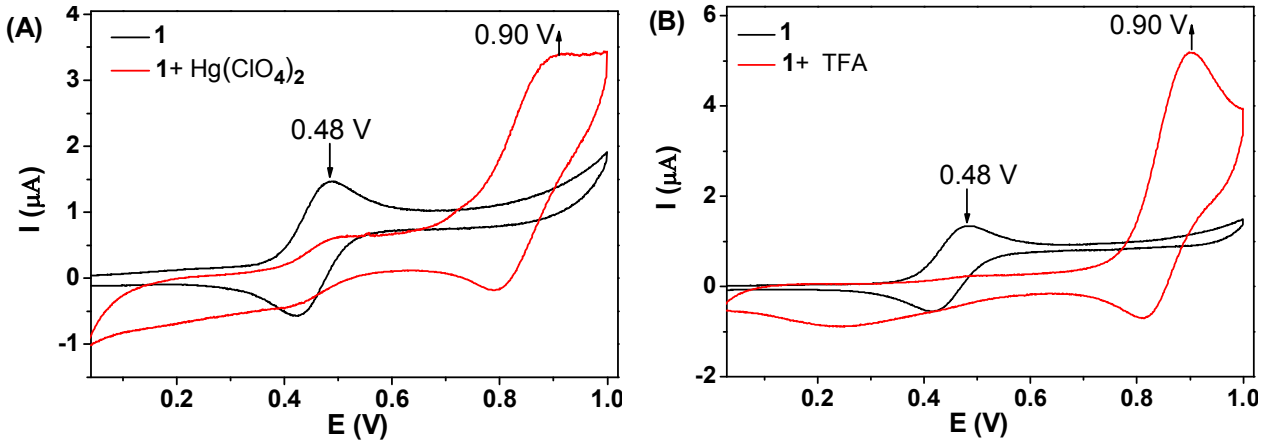

Fig. S8. Cyclic voltammograms of **1** (500 μM) in CH_3CN solution in the absence and presence of (A) $Hg(ClO_4)_2$ and (B) TFA. All measurements were carried out in a one-compartment cell under N_2 gas, equipped with a platinum working electrode, a platinum wire counter electrode, and a $Ag/AgNO_3$ (0.1 M) reference electrode. The supporting electrolyte was 0.10 M tetrabutyl ammonium hexafluorophosphate (Bu_4NPF_6) CH_3CN solution. The potential scan rate was 50 mV/s^{-1}.

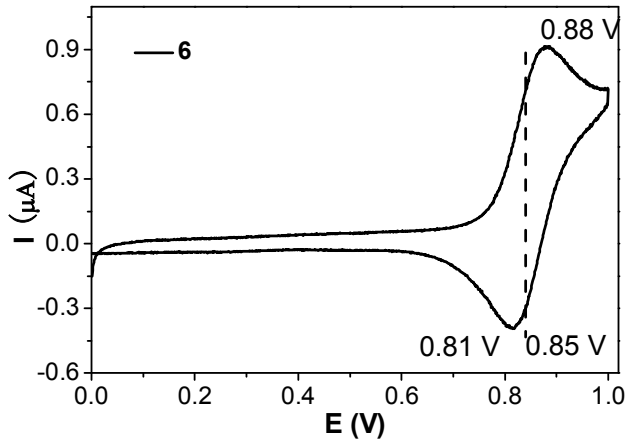

Fig. S9. Cyclic voltammograms of **6** (500 μM) in CH_3CN solution The supported electrolyte was 0.10 M tetrabutyl ammonium hexafluorophosphate (Bu_4NPF_6) CH_3CN solution. The potential scan rate was 50 mV/s^{-1}.

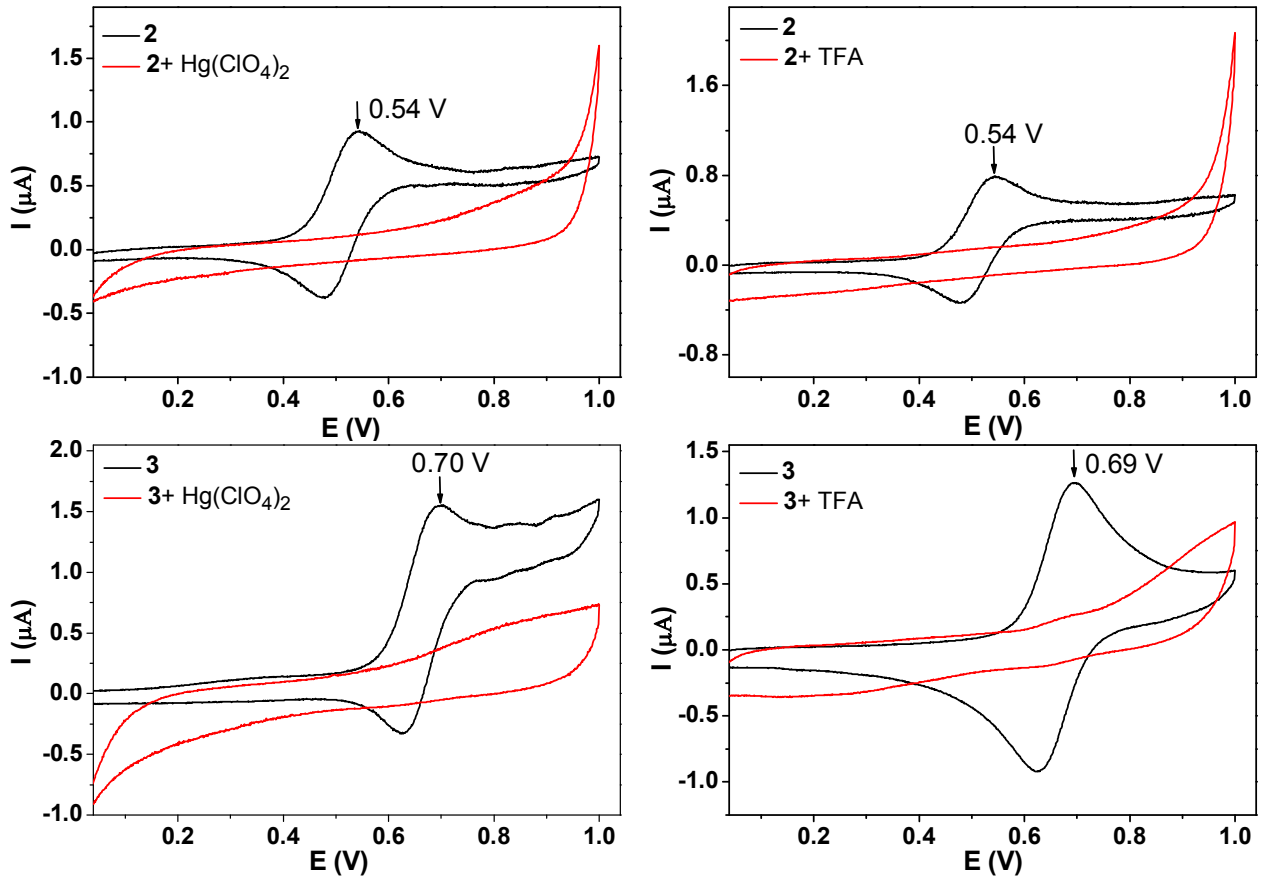

Fig. S10. Cyclic voltammograms of **2** and **3** (500 μM) in CH_3CN solution in the absence and presence of $Hg(ClO_4)_2$ and TFA. The experimental conditions were same as that described in Fig. S8.

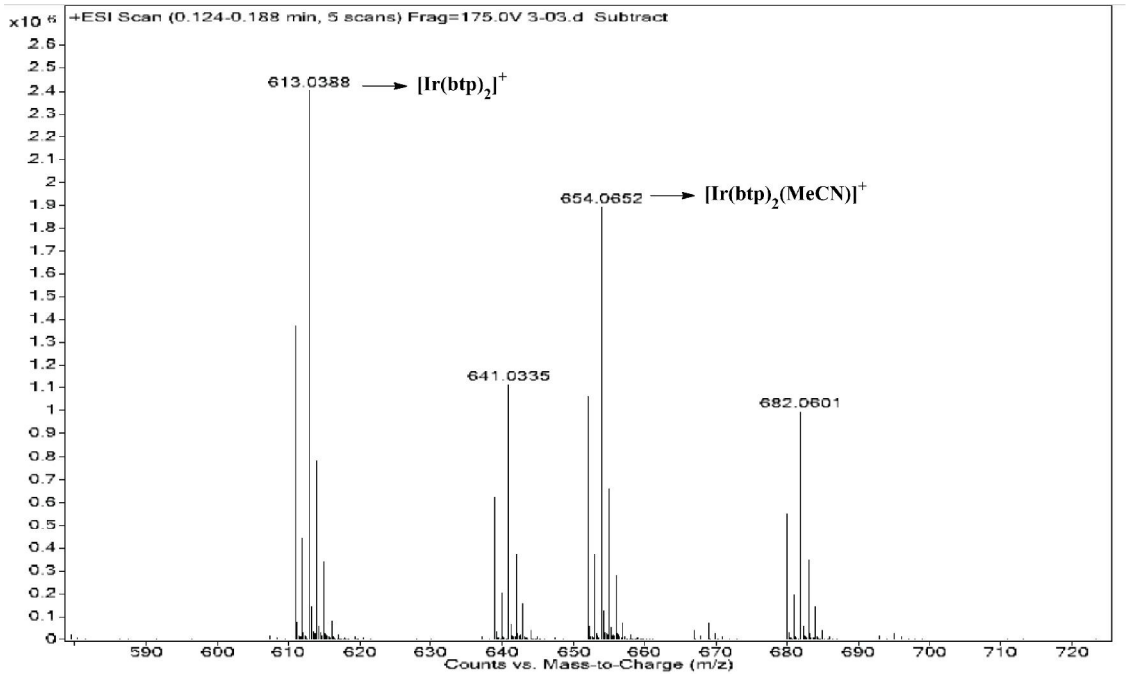

Fig. S11. ESI-MS study of the product of Ir(btp)$_2$acac mixed with 2 equiv of Hg(ClO$_4$)$_2$. The ESI-MS is identical to that of **6**, i,e., [Ir(btp)$_2$(MeCN)$_2$][OTf] synthesized in this work (see Fig. S23).

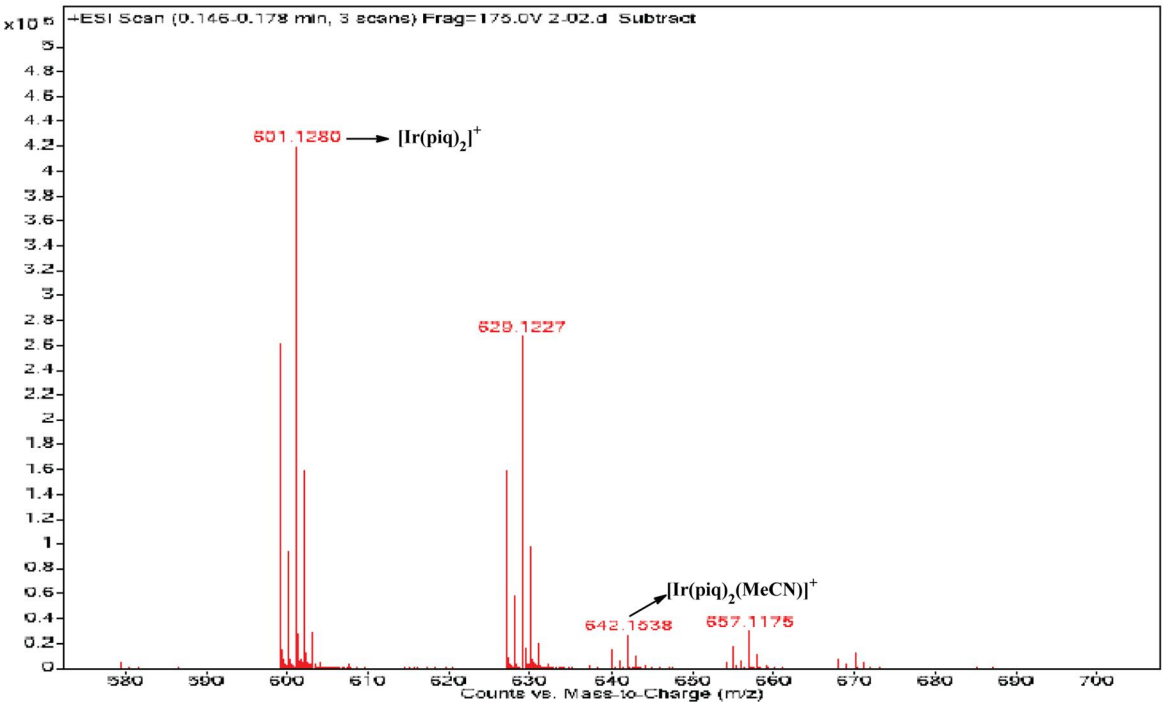

Fig. S12. ESI-MS study of Ir(piq)$_2$acac mixed with 2 equiv of Hg(ClO$_4$)$_2$. The ESI-MS is identical to that of **7**, i,e., [Ir(piq)$_2$(MeCN)$_2$][OTf] synthesized in this work (see Fig. S27).

These studies shown in Fig. S11 & S12 were carried out in order to find any clue of the so-called Hg^{2+}-Ir(btp)$_2$(acac) complex.

Study on the chemical kinetics: The chemical kinetics experiment was measured quantitatively by monitoring the change in absorbance at 476 nm. The cyclometalated Ir(III) complex, $Ir(btp)_2acac$, was dissolved in acetonitrile to obtain a stock solution (150 μM). To 2.5 mL of the Ir(III) complex solution in a quartz cuvette, 25 μL of the aqueous solution of TFA (7.5×10^{-2} M) was added and consequently examined by UV-Vis absorption spectroscopy. The reaction was investigated at five different temperatures (30 °C, 35 °C, 40 °C, 45 °C and 50 °C) and the UV–Vis absorption spectra were recorded as Figure S13. The concentration of $Ir(btp)_2acac$ solution during the reaction was determined spectrophotometrically at 476 nm according to calibration curve (Fig. S14).

$$Ir(btp)_2acac + TFA + MeCN \rightarrow [Ir(btp)_2(MeCN)_2][CF_3COO] + Hacac$$

C_0:	a	b		
C_t:	a-x	b-x	x	x

$Ir(btp)_2acac$ dissociation reaction is estimated as a second-order reaction. The kinetics of the reaction was calculated according to equation (1): $Rate = \frac{d[P]}{dt} = \frac{dx}{dt} = k[Ir(btp)_2acac][TFA] = k(a-x)(b-x)$, the second-order rate constant k was calculated as the equation (2): $k = \frac{1}{t(a-b)}\ln\left[\frac{b(a-x)}{a(b-x)}\right]$. The k at different temperatures were shown in Table S1. A plot of $\ln k$ *versus* 1/T was linear with negative slope and positive intercept (see Fig. S15). According to Arrhenius equation (3): $\ln k = \ln A - \frac{E_a}{RT}$, the apparent activation energy (E_a) was evaluated as 51.6 kJ· mol^{-1}. In the mean time, according to the equation (4): $\ln k = -\Delta G°/RT = -\Delta H°/RT + \Delta S°/R$, $\Delta H°$ and $\Delta S°$ were evaluated as 51.6 kJ· mol^{-1} and 41.7 kJ· mol^{-1} respectively.

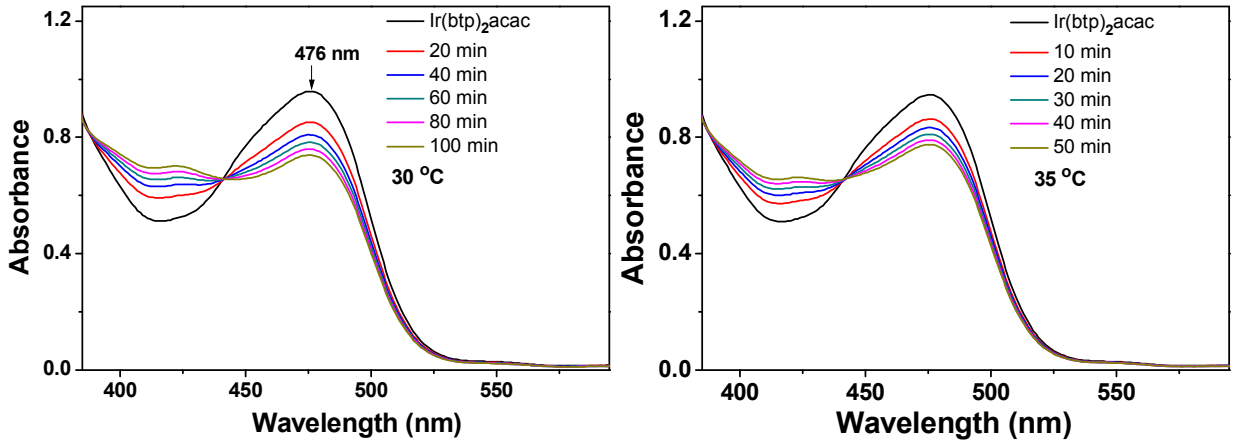

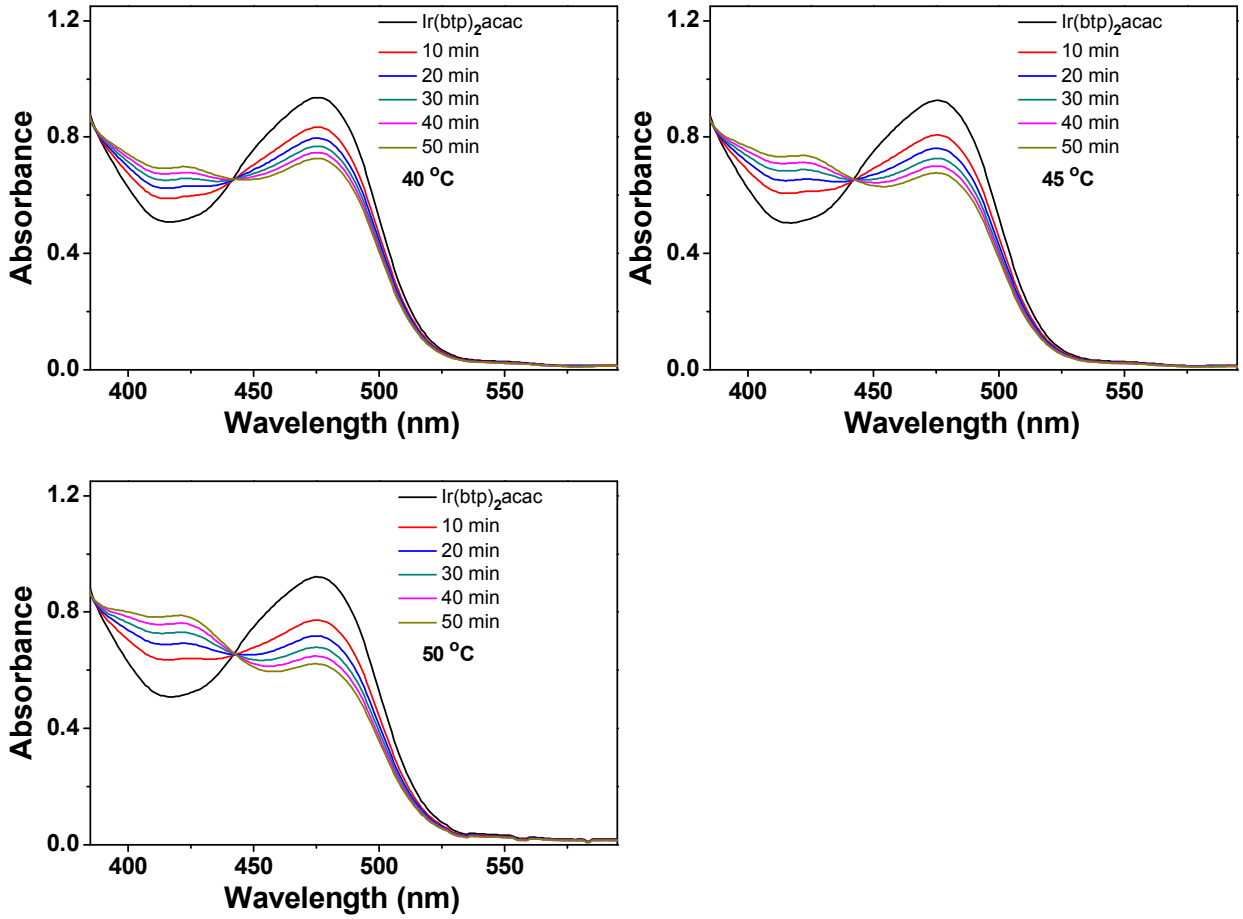

Fig. S13. Absorbance changes with time and temperatures during the reaction of complex $Ir(btp)_2acac$ (150 μM) in CH_3CN solution with 5 eq TFA.

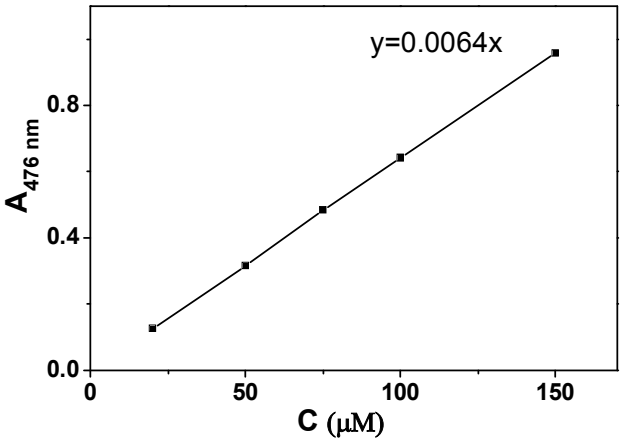

Fig. S14. Representative calibration curve of $A_{476\ nm}$ versus of the concentration of $Ir(btp)_2acac$ in CH_3CN solution.

T (^{o}C)	k (mol^{-1}· L· min^{-1})
30	8.09
35	9.59
40	12.7
45	15.9
50	20.0

Table. S1. k values at different temperatures.

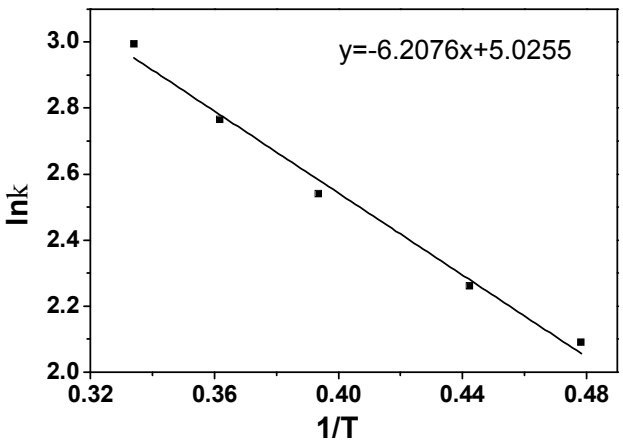

Fig. S15. Plot of ln*k* *vs* 1/T for $Ir(btp)_2acac$

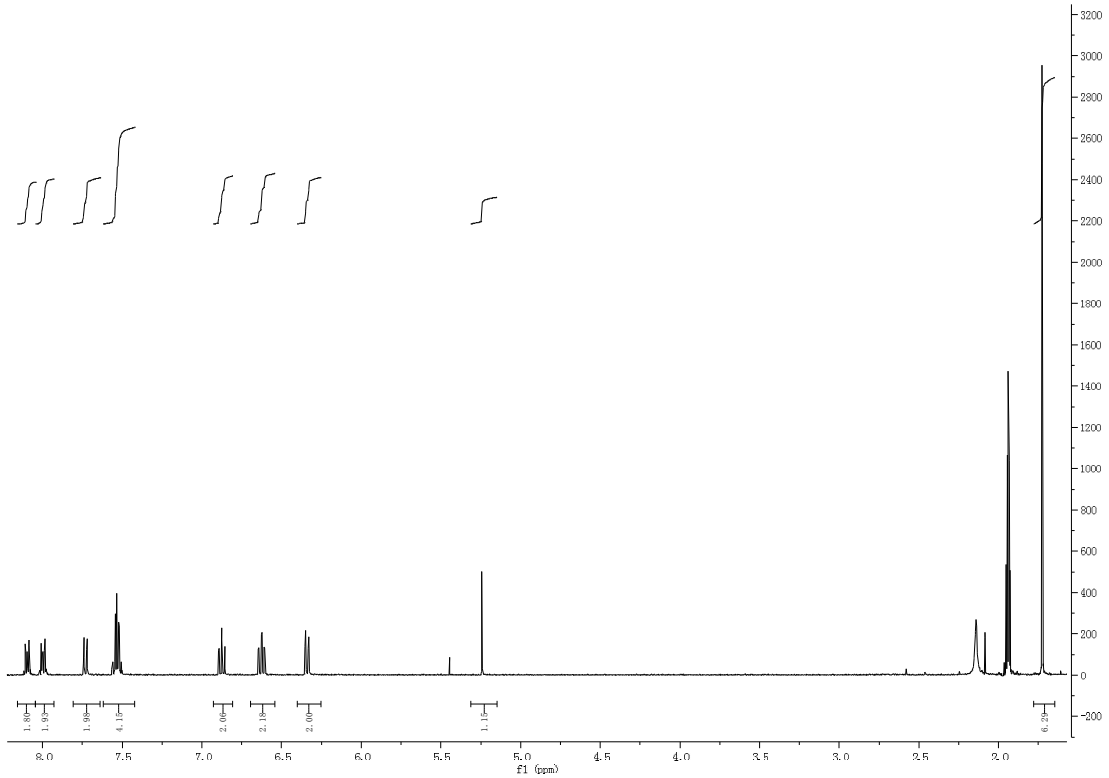

Fig. S16. ^1H NMR spectrum of **3**, i.e., $Ir(bt)_2(acac)$ in CD_3CN

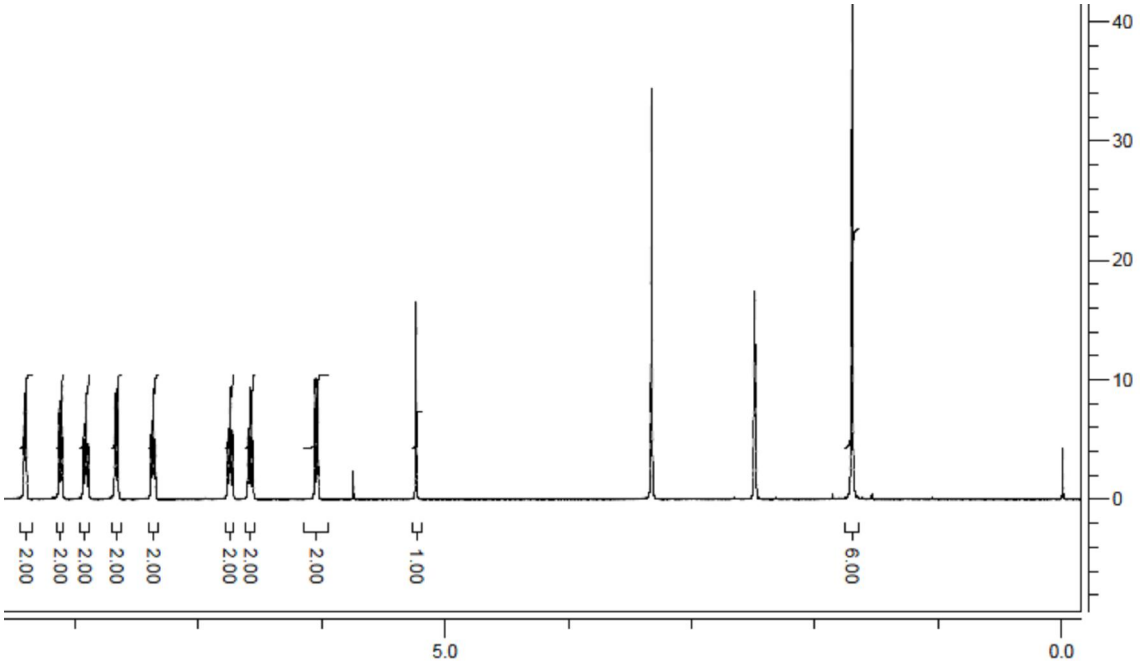

Fig. S17. ^{1}H NMR spectrum of **4**, i.e., Ir(ppy)$_2$(acac) in DMSO-d_6

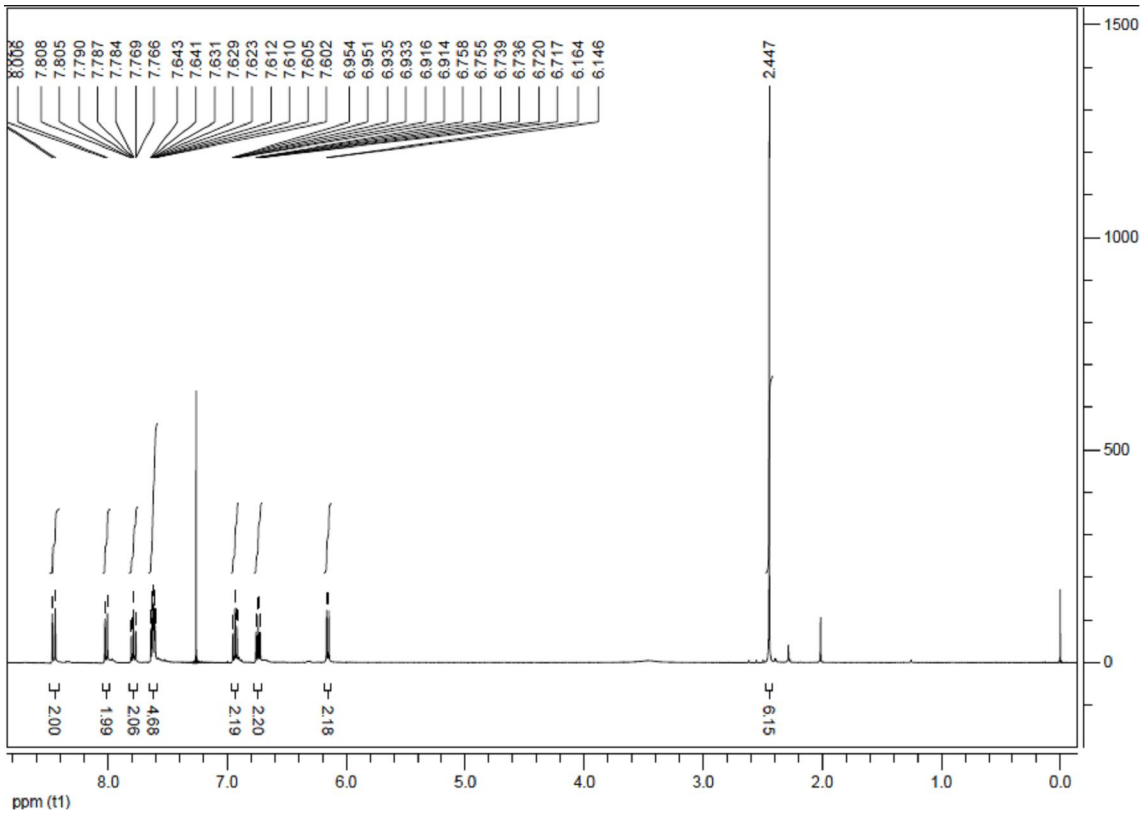

Fig. S18. ^{1}H NMR spectrum of **8**, i.e., [Ir(bt)$_2$(MeCN)$_2$][OTf] in $CDCl_3$.

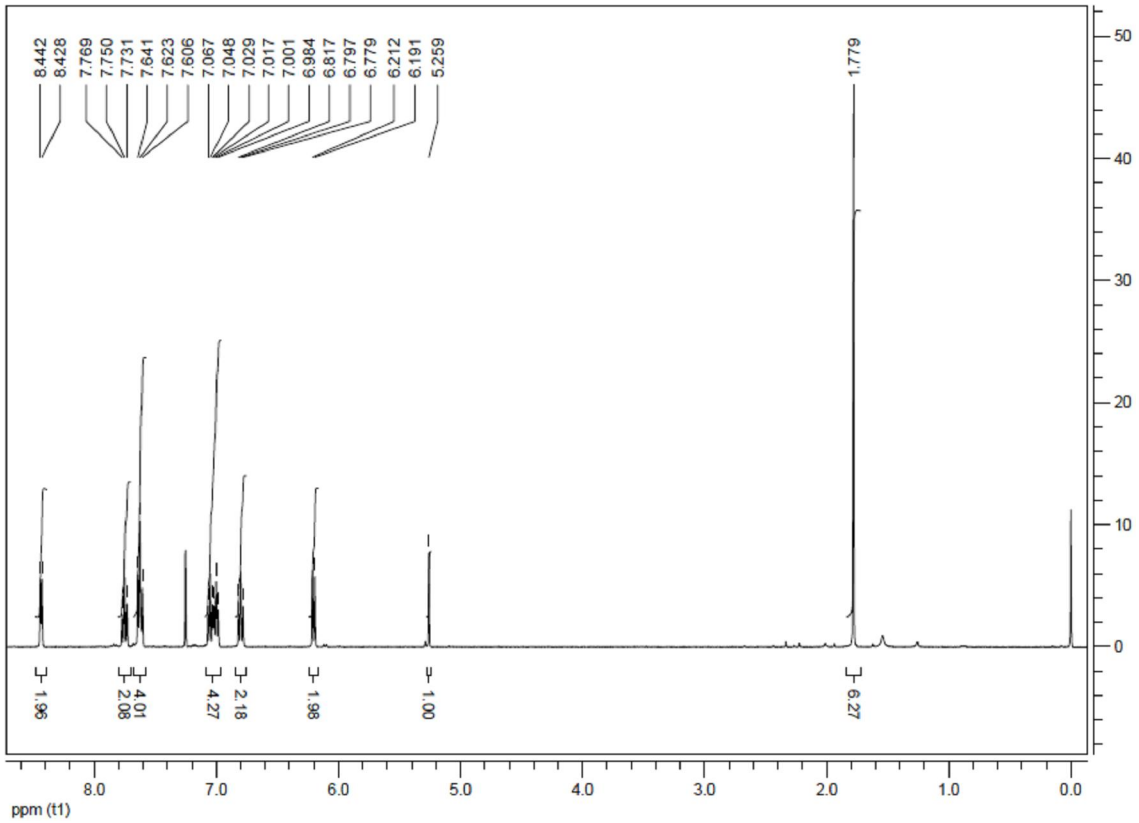

Fig. S19. ^{1}H NMR spectrum of **1**, i.e., $Ir(btp)_2(acac)$ in $CDCl_3$

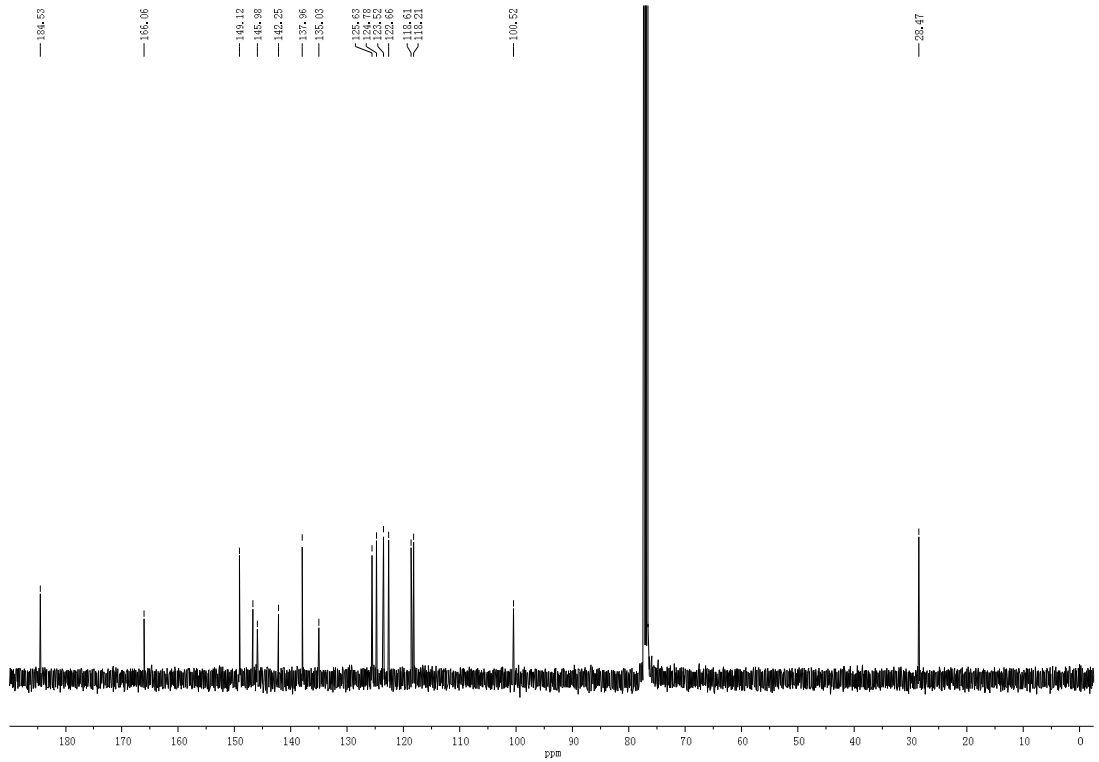

Fig. S20. ^{13}C NMR spectrum of **1**, i.e., $Ir(btp)_2(acac)$ in $CDCl_3$

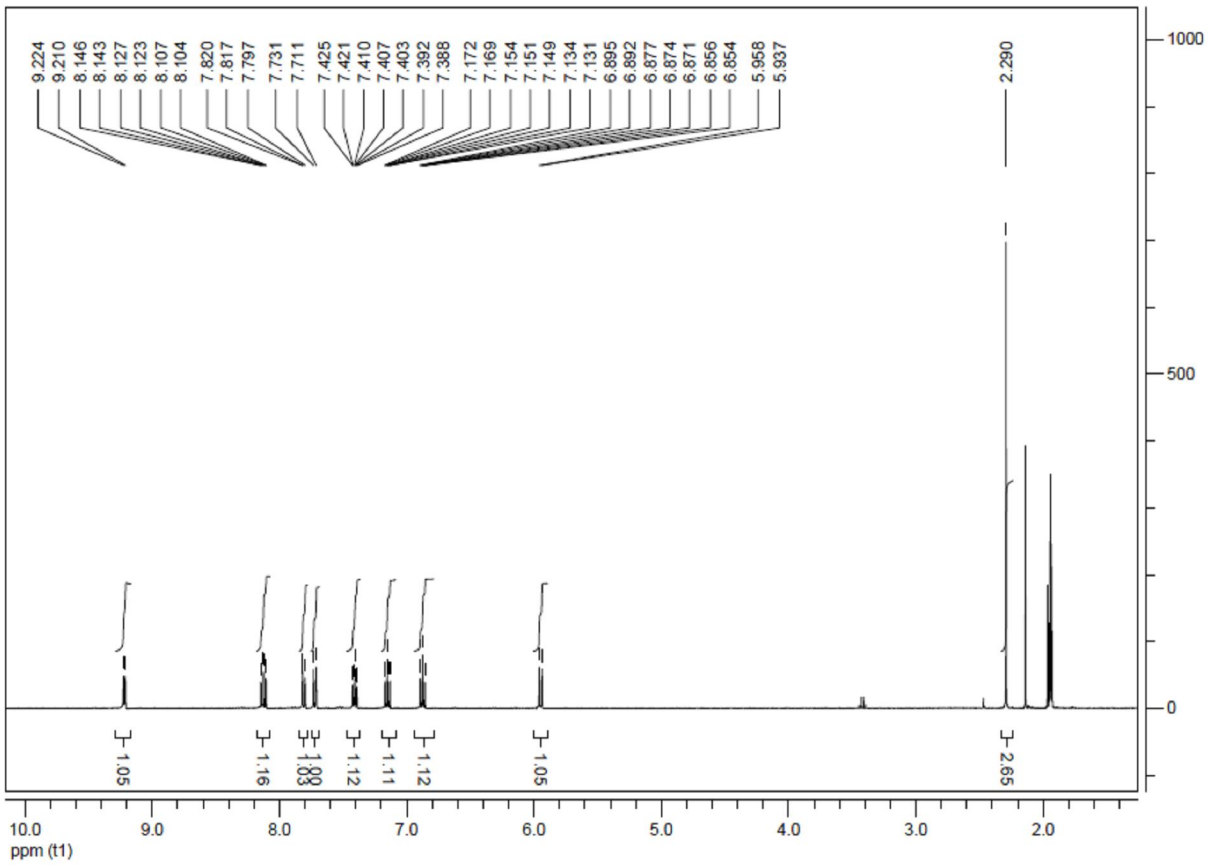

Fig. S21. ^{1}H NMR spectrum of **6**, i.e., $[Ir(btp)_2(MeCN)_2][OTf]$ in CD_3CN

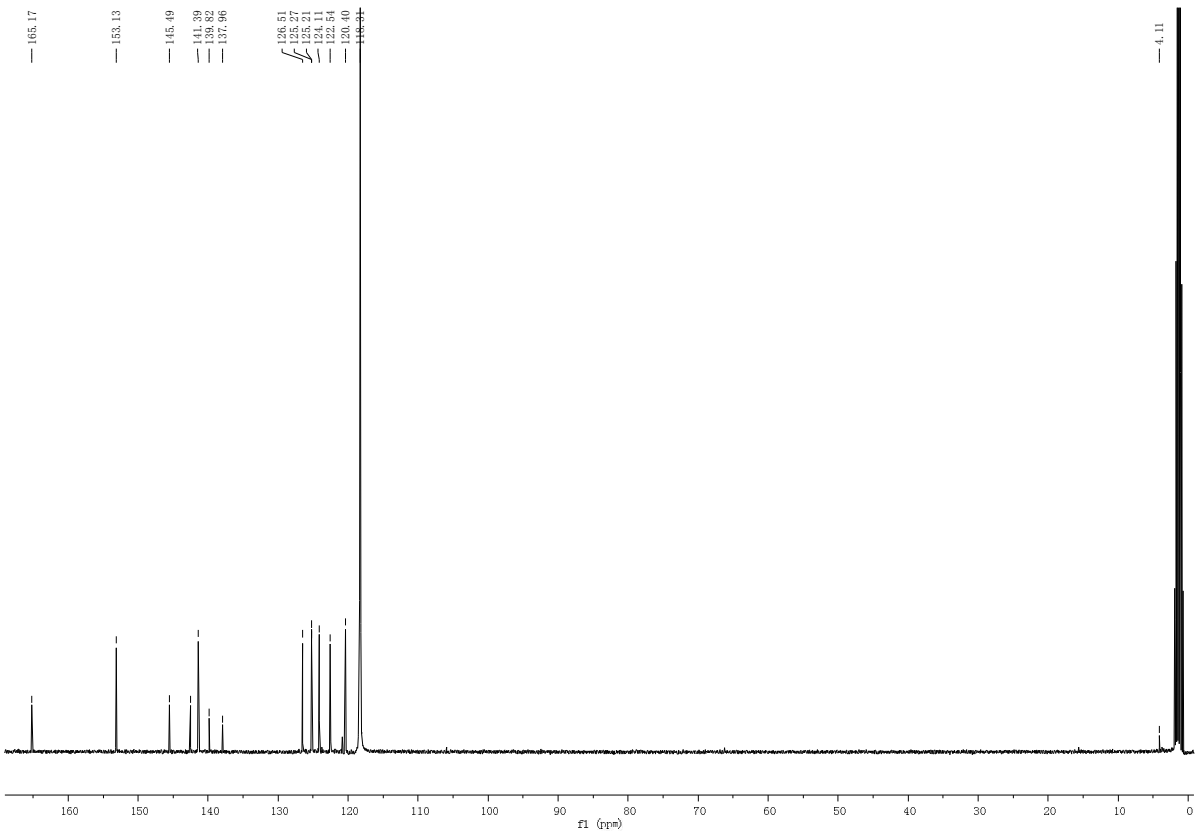

Fig. S22. ^{13}C NMR spectrum of **6**, i.e., $[Ir(btp)_2(MeCN)_2][OTf]$ in CD_3CN

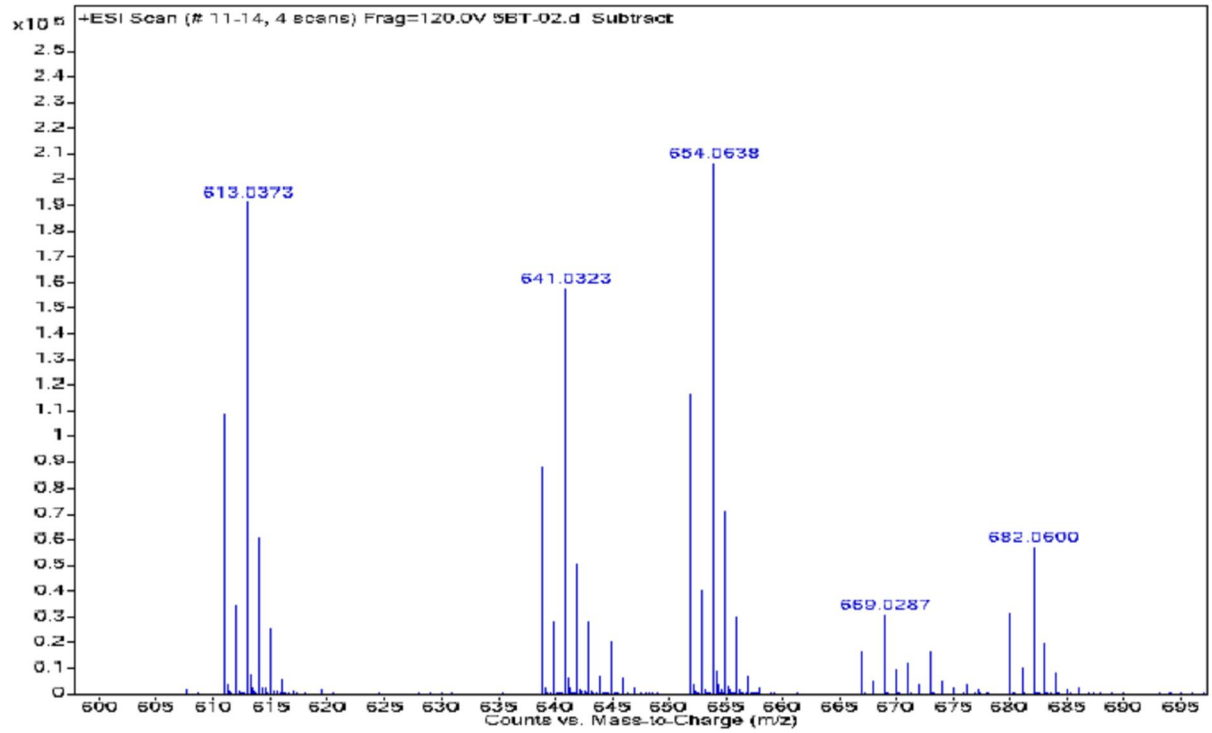

Fig. S23. MS spectra of **6**, i.e., $[Ir(btp)_2(MeCN)_2][OTf]$

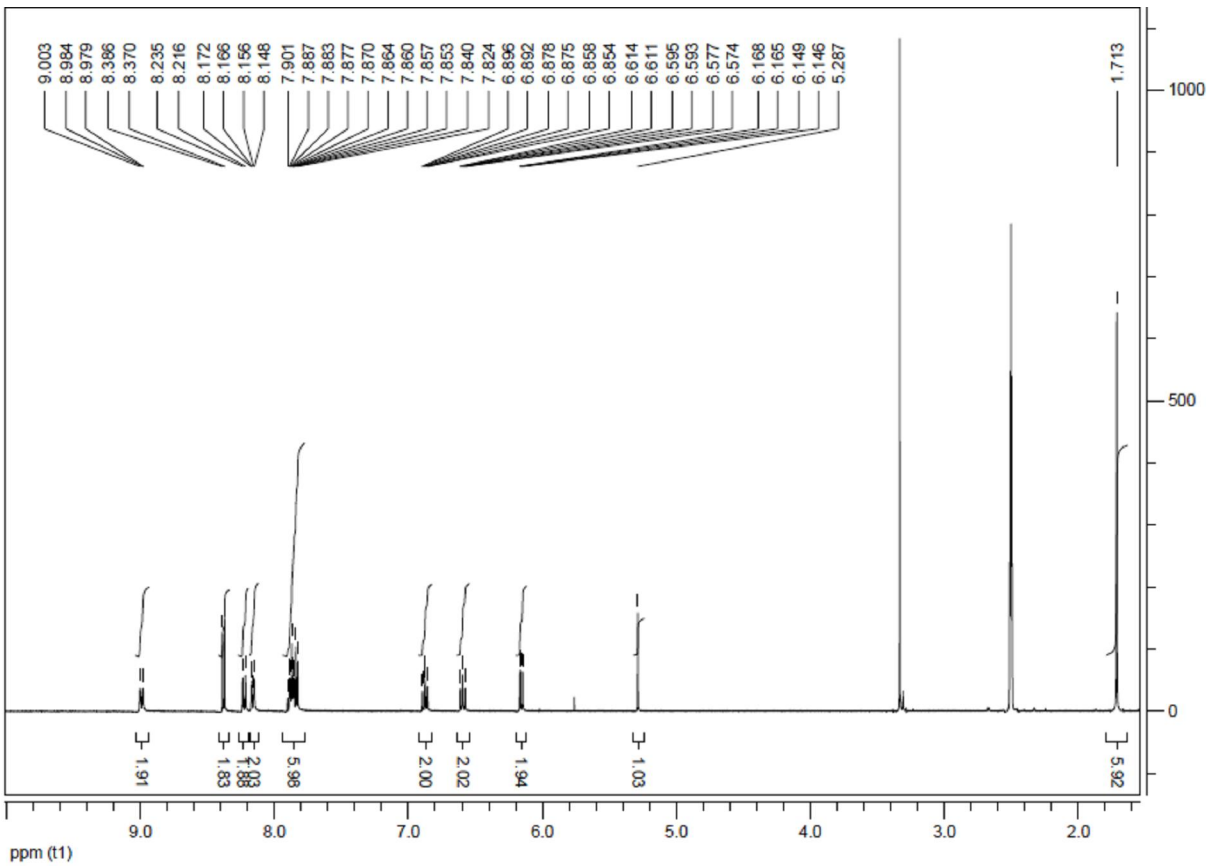

Fig. S24. ^{1}H NMR spectrum of **2**, i,e., $Ir(piq)_2(acac)$ in DMSO-d_6

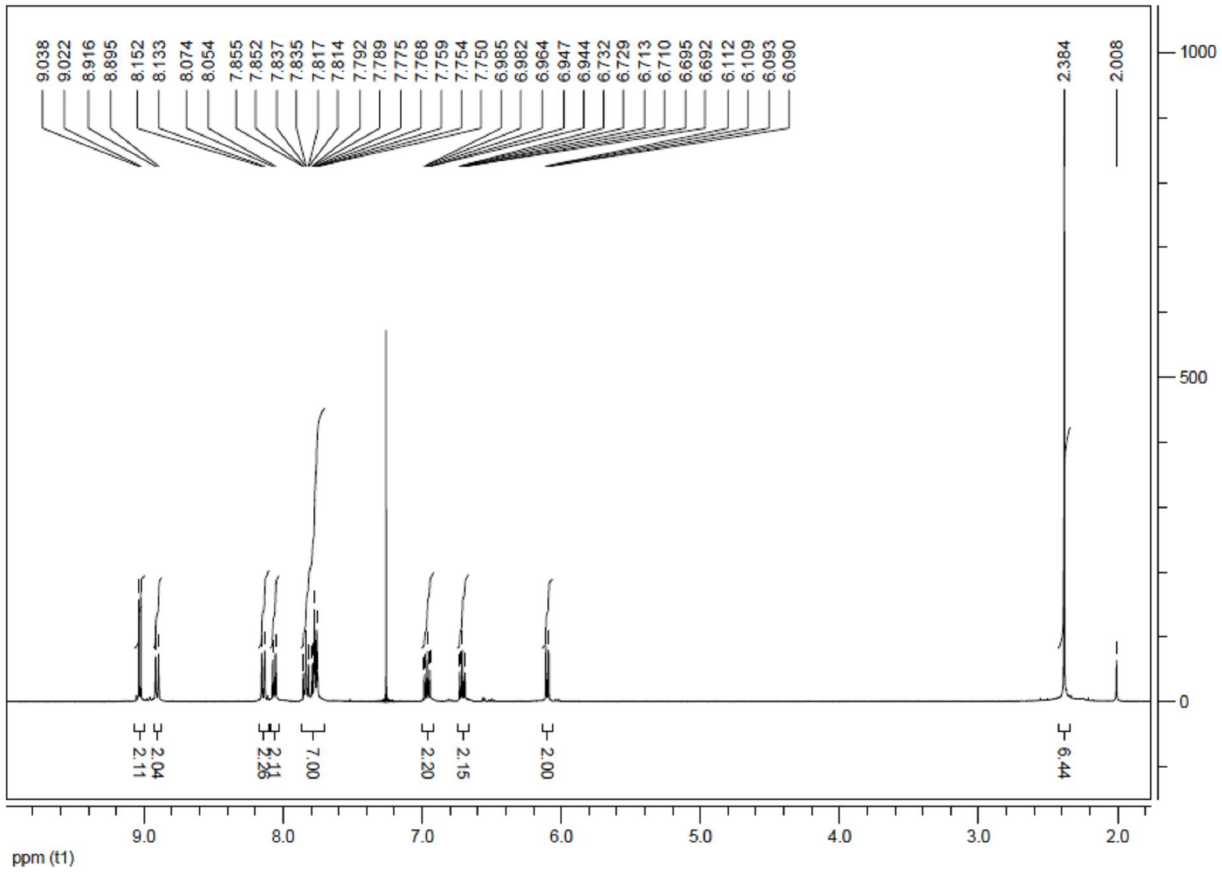

Fig. S25. ^{1}H NMR spectrum of **7**, i,e., $[Ir(piq)_2(MeCN)_2][OTf]$ in $CDCl_3$

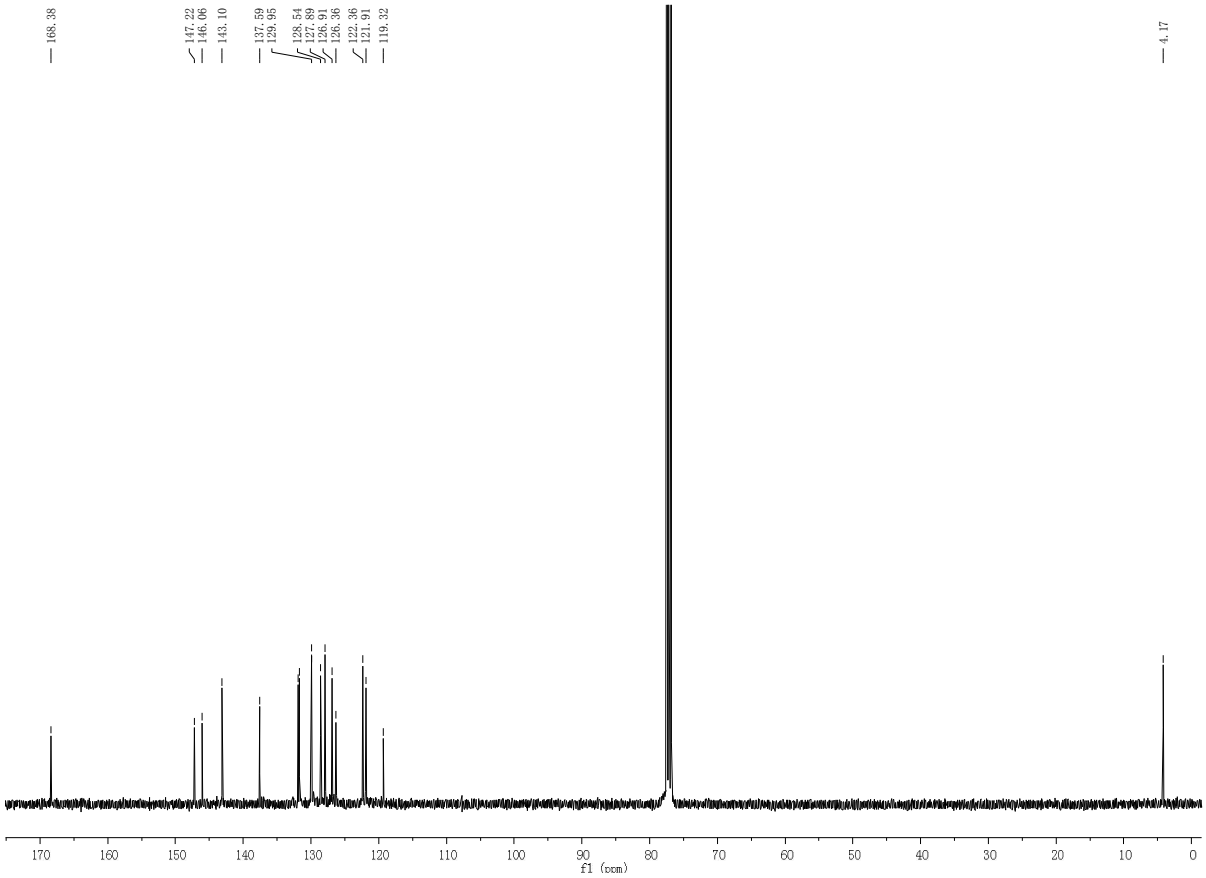

Fig. S26. ^{1}H NMR spectrum of **7**, i,e., $[Ir(piq)_2(MeCN)_2][OTf]$ in $CDCl_3$

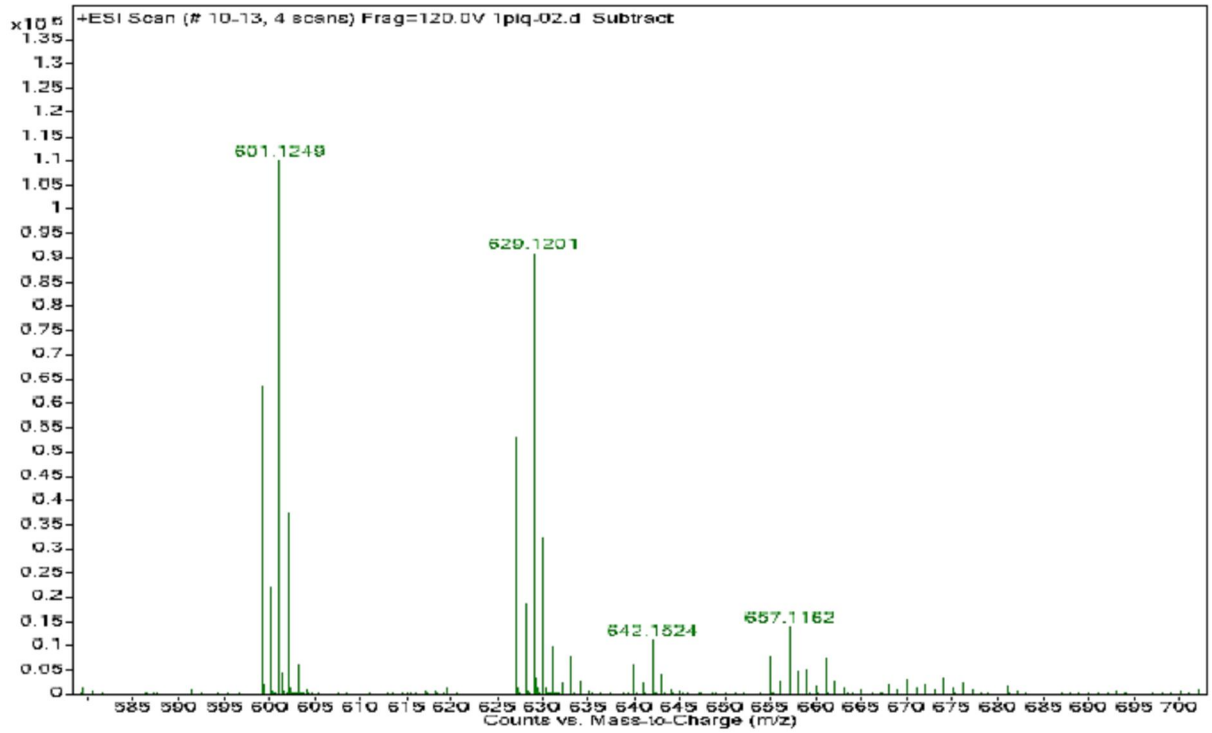

Fig. S27. MS spectrum of **7**, i,e., $[Ir(piq)_2(MeCN)_2][OTf]$.

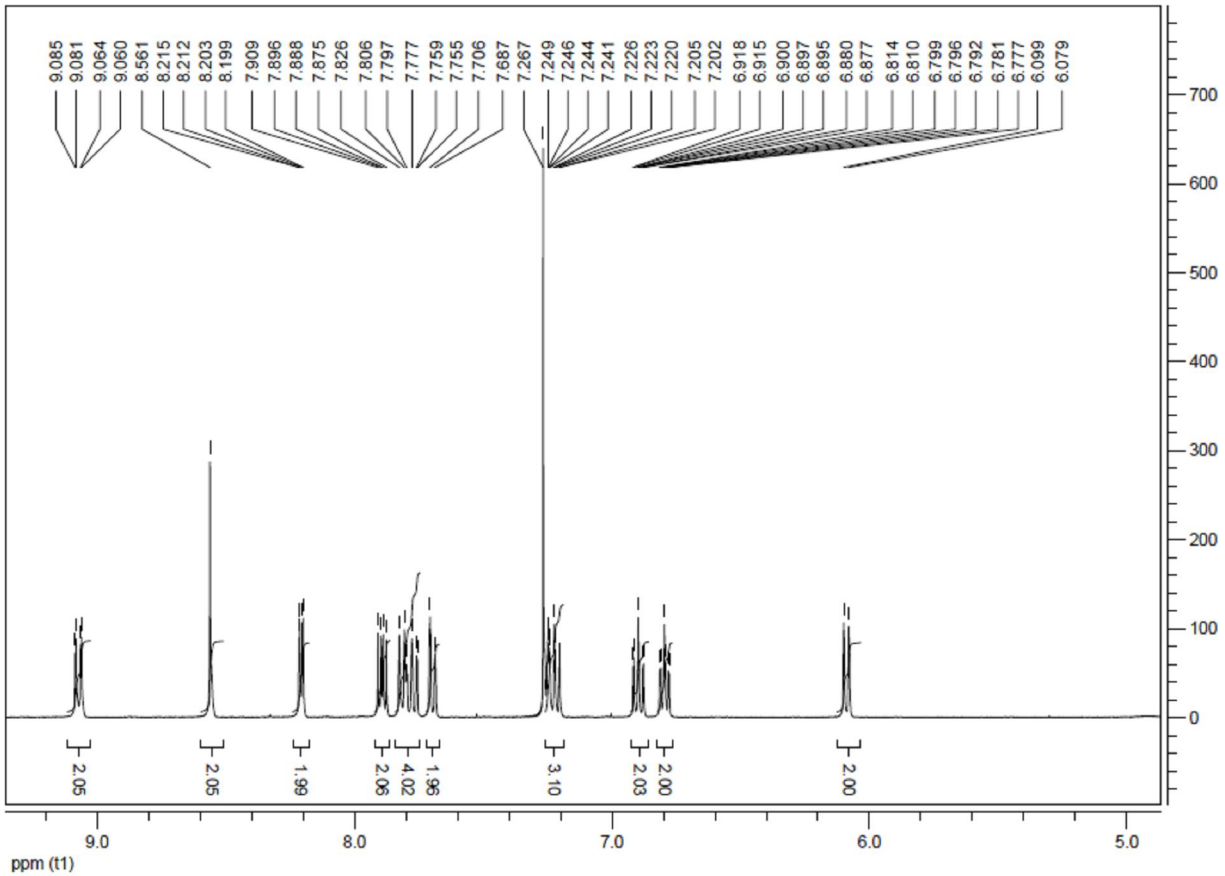

Fig. S28. ^1H NMR spectrum of **5**, i.e., $[Ir(btp)_2(phen)][Cl]$ in $CDCl_3$

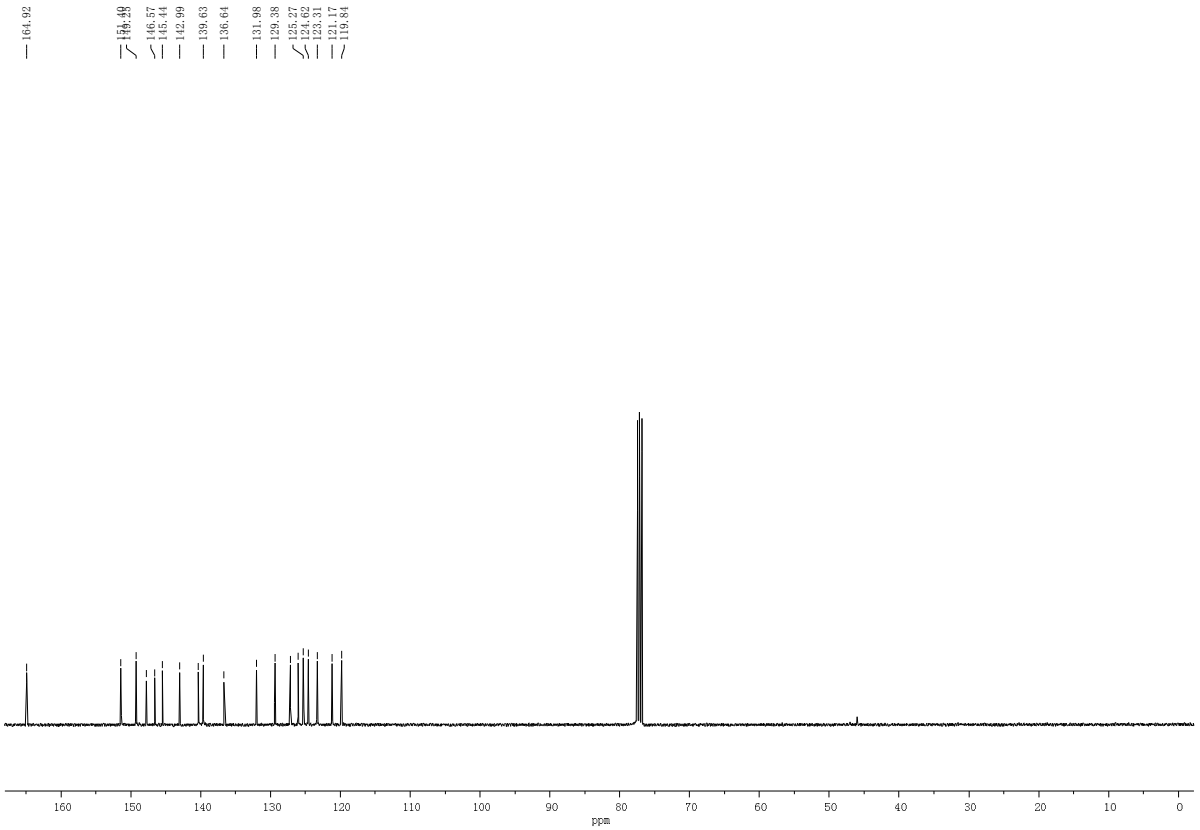

Fig. S29. ^{13}C NMR spectrum of **5**, i.e., $[Ir(btp)_2(phen)][Cl]$ in $CDCl_3$

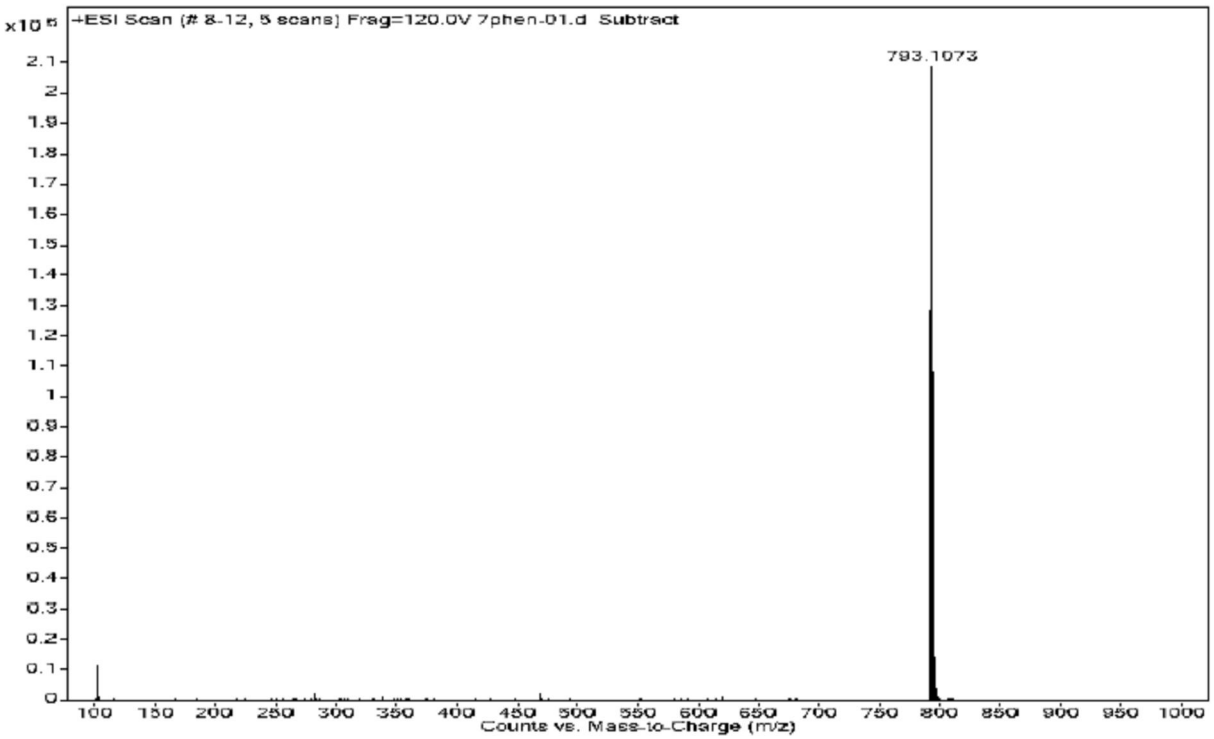

Fig. S30. MS spectrum of **5**, i.e., $[Ir(btp)_2(phen)][Cl]$.